Journal of Quantitative Spectroscopy & Radiative Transfer 248 (2020) 106963

Contents lists available at ScienceDirect

Journal of Quantitative Spectroscopy & Radiative Transfer

journal homepage: www.elsevier.com/locate/jqsrt

Absolute frequency metrology of the CHF_3 8.6-μm ro-vibrational spectrum at 10^{-11} level

Edoardo Vicentini[a,b], Pasquale Maddaloni[c,d], Roberto Aiello[c], Alessio Gambetta[a,b], Nicola Coluccelli[a,b], Lisa M. Molteni[a,b], Antonio Castrillo[e], Livio Gianfrani[e], Paolo De Natale[f,g], Paolo Laporta[a,b], Gianluca Galzerano[a,b,*]

[a] Dipartimento di Fisica - Politecnico di Milano, Piazza Leonardo da Vinci 32, 20133 Milano, Italy
[b] Istituto di Fotonica e Nanotecnologie - CNR, Piazza Leonardo da Vinci 32, 20133 Milano, Italy
[c] Istituto Nazionale di Ottica - CNR, Via Campi Flegrei 34, 80078 Pozzuoli (NA), Italy
[d] INFN, Istituto Nazionale di Fisica Nucleare, Sez. di Napoli, Complesso Universitario di M.S. Angelo, Via Cintia, 80126 Napoli, Italy
[e] Dipartimento di Matematica e Fisica - Università degli Studi della Campania "Luigi Vanvitelli", Viale Lincoln 5, 81100 Caserta, Italy
[f] Istituto Nazionale di Ottica - CNR, Largo E. Fermi, 6, 50125 Firenze, Italy
[g] INFN, Istituto Nazionale di Fisica Nucleare, Sez. di Firenze, Via G. Sansone 1, 50019 Sesto Fiorentino, Italy

ARTICLE INFO

Article history:
Received 20 February 2020
Revised 14 March 2020
Accepted 14 March 2020
Available online 21 March 2020

Keywords:
Wavelength-modulation Lamb-dip spectroscopy
Optical-frequency-comb-assisted absolute frequency metrology
CHF_3 ro-vibrational spectrum

ABSTRACT

An optical-frequency-comb-referenced quantum cascade laser is used to perform wavelength-modulation Lamb-dip spectroscopy on a large number of ro-vibrational transitions falling in the CHF_3 υ_5 fundamental band at 8.6 μm. The combined (statistical + systematic) fractional uncertainty in the absolute determination of the line-center frequencies ranges from 9×10^{-11} down to 2×10^{-11}. This represents an improvement by more than two orders of magnitude, as compared to a recent and extensive study performed with a high-resolution FTIR spectrometer [1]. Our investigation realizes a sharpened knowledge of the CHF_3 spectrum over a wide interval, also managing to accurately determine the positions of very close, previously unresolved multiple ro-vibrational components.

1. Introduction

Fluoroform (trifluoromethane, CHF_3) plays a key role in different areas of physics and chemistry, both from a fundamental and an applied perspective: it is a significant pollutant and greenhouse gas [2]; it represents a prototype for the study of intramolecular quantum dynamics as well as for ^{13}C isotope separation [3,4]; it is a target in the field of cold stable molecules, promising novel applications ranging from quantum simulations to controlled reactions [5]. For these reasons, the CHF_3 molecule has become the subject of a new line of spectroscopic studies with increasingly higher resolution levels. In this framework, a major effort has been recently undertaken to remeasure the entire infrared spectrum of fluoroform at the highest resolution currently available by Fourier Transform Infrared (FTIR) spectroscopy (30 MHz) [1].

In this work, we use an optical-frequency-comb-referenced quantum cascade laser to perform wavelength-modulation Lamb-dip spectroscopy on a huge number of ro-vibrational transitions belonging to the CHF_3 υ_5 fundamental band (asymmetric F-C-F bending) at 8.6 μm, reaching a best combined (statistical + systematic) uncertainty in the line-center frequency determination as low as 640 Hz (2×10^{-11} in fractional terms). This represents a two-order-of-magnitude improvement compared to our latest investigation in the same spectral interval, by virtue of significant upgrades made to the previously developed spectrometer [6].

2. Experimental apparatus

The sub-Doppler wavelength modulation (WM) spectroscopy setup is shown in Fig. 1. As discussed in detail in a previous work [6], the spectrometer is based on a continuous-wave QCL tunable in the wavenumber range from 1156 to 1160 cm^{-1} (34.68–34.80 THz).

The QCL output beam, linearly polarized along the vertical direction, is focused inside an optical isolator (isolation > 25 dB) and then power split by an uncoated ZnSe window placed at the Brewster angle. The reflected beam, linearly polarized orthogonal to the incidence plane, is sent, passing through a quarter waveplate (QWP), to the gas cell (25-cm long), whereas the transmitted beam serves for absolute frequency calibration using a mid-infrared op-

* Corresponding author.
E-mail address: gianluca.galzerano@polimi.it (G. Galzerano).

https://doi.org/10.1016/j.jqsrt.2020.106963
0022-4073/

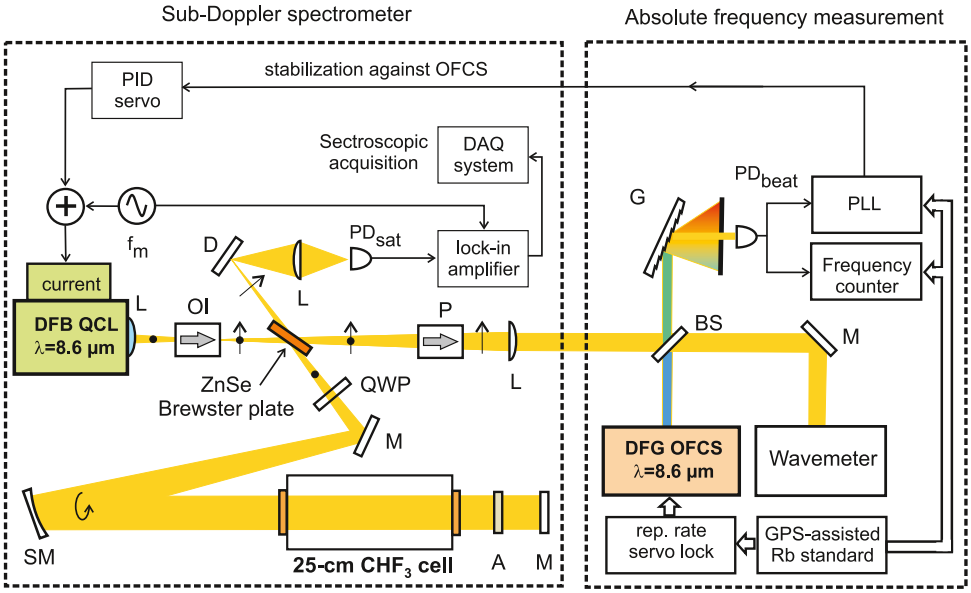

Fig. 1. Experimental setup for CHF_3 saturated absorption spectroscopy and absolute frequency measurements. The dots and arrows in the beam represent, respectively, the vertical and horizontal linear polarization states (counterclockwise arrow represent circular polarization state). A: optical attenuator; BS: beam splitter; D: diffuser; DAQ: data acquisition system; G: diffraction grating; L: lens; M: gold mirror; SM: spherical mirror; OI: optical isolator; P: polarizer; PD: photodetector; PID: proportional-integrative-derivative servo; PLL: phase-locked-loop servo; QWP: quarter waveplate.

tical frequency comb (MIR OFC). The latter is produced via difference frequency generation (DFG) in a GaSe nonlinear crystal between two pulse trains at 1.55 and 1.89 μm wavelengths, respectively, coming from a dual-branch 250-MHz femtosecond Er:fiber laser system [7]. The realized harmonic MIR OFC (the offset frequency cancels out in the DFG process) operates at a central wavelength of 8.6 μm with an average output power of 4 mW and an optical bandwidth of 0.8 μm (corresponding to 0.22 μW per comb tooth) [7]. The link to the Cs frequency primary standard is eventually established by stabilizing the comb mode spacing (repetition rate) against a GPS-disciplined Rb clock. To phase-lock the QCL to the closest MIR OFC tooth, the beat-note signal from photodetector PD_{beat} is compared, via a fast and low-noise phase detector, to a reference signal at 70 MHz provided by a RF synthesizer synchronized with the Rb standard. The error signal at the phase detector output is then fed back to the QCL current driver through a 1-MHz-bandwidth proportional-derivative-integrative (PID) servo. The RF spectrum of the resulting closed-loop beat-note signal is shown in Fig. 2. In the slow phase-lock control bandwith configuration, it returns a free-running QCL emission linewidth (full width at half maximum) of 250 kHz for observation times of 10 ms. For a phase-lock control bandwidth of ~500 kHz, the beat note signal-to-noise ratio (SNR) increases to 42 dB and its linewidth narrows down to the instrument resolution bandwidth (1 kHz), indicating a tight coherent phase-lock between QCL and MIR OFC. In this case, the QCL emission linewidth corresponds to that of the MIR OFC, which is ~50 kHz, slightly broader than the 21-kHz linewidth of the free-running comb reported in [8] due to the additional phase-noise of the Rb radio-frequency standard we used for MIR OFC stabilization.

To further characterize the stability of the comb-locked QCL, the beat-note frequency is also measured by a reciprocal electronic counter. Fig. 3 shows the corresponding Allan deviation as a function of the counter gate time (integration time) together with the stability of the Rb reference (as measured with respect to a hydrogen maser [9]) used to stabilize the MIR OFC mode spacing. It is worth noting that the measured fractional stability is limited by a white frequency noise contribution equal to $3 \times 10^{-14} \cdot \tau^{-1/2}$, more than one-order of magnitude better than the stability of the Rb-

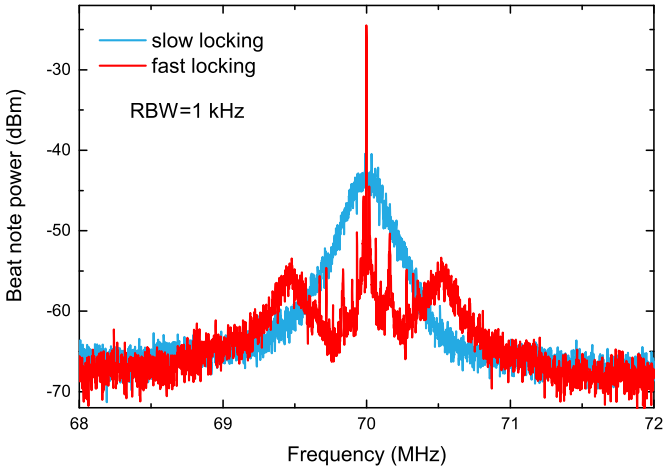

Fig. 2. RF spectrum of the closed-loop beat-note signal between the QCL and the MIR OFC. For a phase-lock control bandwidth of ~500 kHz (as inferred from the servo bumps), a peak with a signal-to-noise ratio (SNR) of 42 dB and a linewidth of 1 kHz (limited by the instrument resolution bandwidth) is observed.

reference (black curve), indicating again a full transfer of the MIR OFC coherence to the QCL. In this way, by tuning the comb mode spacing, the QCL frequency is scanned with the accuracy of the Rb reference.

We implemented a saturated-absorption spectroscopic scheme with circularly polarized pump and probe beams, in a power ratio of 4:1 and with a collimated diameter of 8 mm (corresponding to a transit time line broadening of ~20 kHz), which counter-propagate in a collinear geometry inside the gas cell. The probe beam is then collected by a 10-MHz bandwidth, thermoelectrically-cooled mercury-cadmium-telluride (MCT) photodetector through the transmission of the Brewster ZnSe plate, followed by a metallic diffuser and a plano-convex focusing lens. The combination of the ZnSe Brewster plate and the optical diffuser dramatically reduces parasitic etalon effects in the spectroscopic absorption features. Moreover, in the present setup we pay

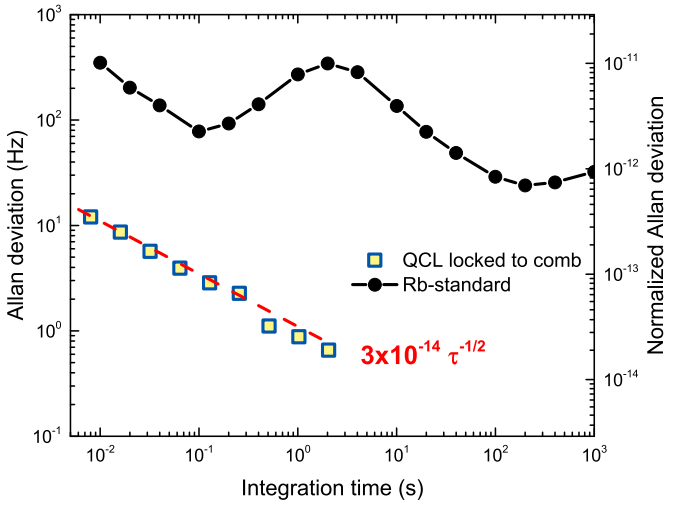

Fig. 3. Allan deviation of the closed-loop beat note between the QCL and MIR OFC, the dashed red curve being the fitted white frequency noise level. The black curve represents the stability of the Rb standard.

specific attention to the design and realization of the absorption cell, in order to reduce gas leakages to a level of 0.5 Pa/h, as measured by a calibrated capacitive pressure transducer (Model Ceravа CTR-100). These two major advances allow to operate at CHF_3 pressures lower than 1 Pa and hence at pump powers as low as $\sim$1 mW. Under these conditions, Lamb-dip line widths (full width at half maximum) narrower than 350 kHz are observed, five times better than what obtained in previous investigations [6,14]. In conjunction with an enhanced SNR, this significantly improves the ultimate accuracy in the line-center frequency determination.

To implement the WM method [10], the QCL driving current is sinusoidally modulated at a frequency of $f_m = 100$ kHz with a depth of $\Delta f = 200$ kHz. Then, in order to determine the line-center frequency of the observed WM dispersion-like Lamb-dip profiles (in-phase first-harmonic demodulated signals), the following scheme is used. Following phase-locking of the QCL to the closest MIR OFC tooth, the QCL frequency can be scanned across the molecular resonance by finely tuning the comb mode spacing; the line-center frequency is eventually retrieved by numerical interpolation of the dispersion-like Lamb-dip signal.

3. Spectroscopic results

As an example, Fig. 4(a) shows the first-harmonic WM signal corresponding to ${}^rR_{40}(64)$ ro-vibrational line (in the υ_5 fundamental band), recorded at a saturating pump power of 1.2 mW and for different CHF_3 pressures ranging from 0.1 to 8.3 Pa. For each Lamb-dip profile, the line-center frequency is obtained by a numerical fitting using the following equation [11]

$$S_{WM}(\omega) = \left[S_{1,D}(\omega) + S_{1,SD}(\omega)\right] \tag{1}$$

where $S_{1,D}$ and $S_{1,SD}$ are the first-order in-phase lock-in output signals relative to the Doppler-broadened absorption profile and the sub-Doppler absorption Lamb-dip feature. In general, each of these signals can be expressed as [11]

$$S_1 = A\,\overline{\chi}_1 + B\,(3\,\overline{\chi}_0 + \overline{\chi}_2) + C\,\overline{\chi}_3 \tag{2}$$

where A, B and C are suitable coefficients, and $\overline{\chi}_n$ (with $n = 0, 1, 2, 3$) represents the even component of the n-th Fourier coefficient of the wavelength-modulated peak-normalized absorption lineshape function $\overline{\chi}(\overline{\omega}_d, \overline{\omega}_a, t)$ [12]:

$$\overline{\chi}_n(\overline{\omega}_d, \overline{\omega}_a) = \frac{2 - \delta_{n0}}{1/\Omega_m} \int_0^{1/\Omega_m} \overline{\chi}(\overline{\omega}_d, \overline{\omega}_a, t)\cos(2\pi n\,\Omega_m t)\,dt \tag{3}$$

Here, δ_{n0} is the Kronecker delta, Ω_m is the modulation frequency, ω_0 is the line-center frequency, $\overline{\omega}_d = (\omega - \omega_0)/\Delta\omega$, $\overline{\omega}_a = a_m/\Delta\omega$, and $\Delta\omega$ is the linewidth of the absorption profile. It is worth pointing out that Eq. 2 also takes into account the distortion introduced in the signal by residual amplitude modulation through the zero, second, and third Fourier coefficients of the lineshape function [13]. In our model, a simple linear function is adopted for the Doppler-broadened absorption profile, whereas a Voigt lineshape function is used for the sub-Doppler absorption Lamb dip.

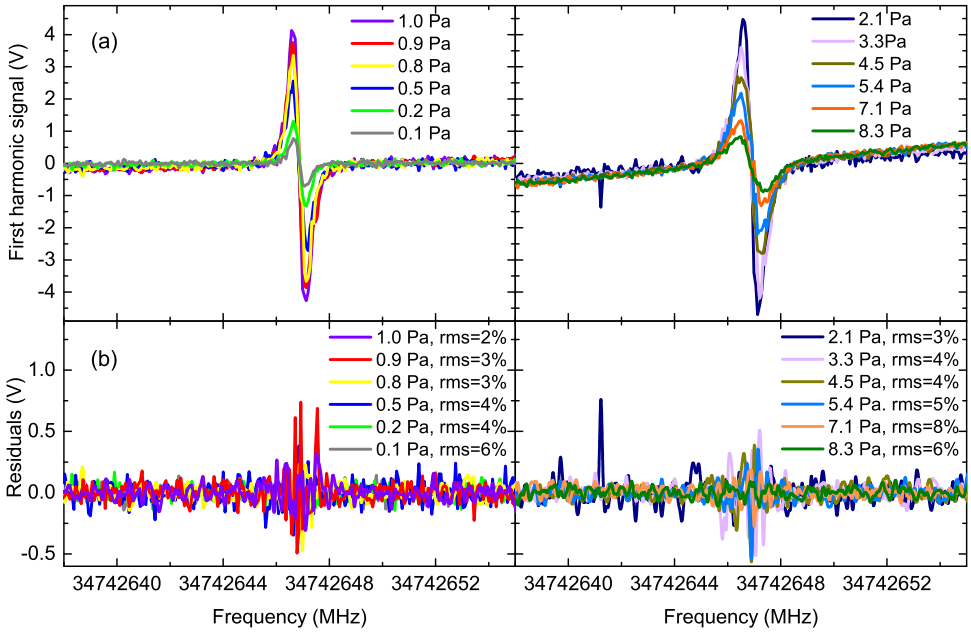

Fig. 4. (a) First-harmonic WM signal corresponding to the ${}^rR_{40}(64)$ line, recorded for a saturating pump power of 1.2 mW and for different CHF_3 pressures (30-ms lock-in integration time). (b) Fit residuals obtained using Eq. (1), assuming a Voigt line-shape profile for the sub-Doppler absorption Lamb dip and a linear function for the Doppler-broadened background absorption.

Table 1
Summary of estimated systematic uncertainties associated with the absolute determination of the center frequency of the $^{r}R_{40}(64)$ transition.

Source	Coefficient	Uncertainty (kHz)
CHF_3 pressure	-5(2) kHz/Pa	0.3
Pump power	<1 kHz/mW	<0.1
Beam steering and etalon effects	10 kHz/mrad	0.2
Modulation depth	<10 kHz/100 kHz	negligible
Rb-clock		0.08
Total contribution		0.4 (1×10^{-11} in relative terms)

Table 2
Absolute center frequencies of several ro-vibrational lines in the CHF_3 υ_5 band, measured for a gas pressure of 1 Pa and pump power of 1.2 mW. Comparison is made with the values measured with a frequency resolution of 30 MHz by S. Albert and co-workers for a gas pressure of 5 Pa [1]. The reported uncertainties correspond to the type A statistical contribution (1-sigma) that has to be combined with an estimated type B uncertainty on the order of 400 Hz (as deduced by Table 1).

	Line	FTIR [1] (MHz)	This work (MHz)	FTIR - This work (MHz)
1	$^{r}R_1(1)$	34 708 835.2	34 708 837.8290 ± 0.0017	−2.656
2	$^{r}R_2(2)$	34 712 895.6	34 712 899.8615 ± 0.0013	−4.299
3	$^{r}R_3(3)$	34 716 957.2	34 716 956.0149 ± 0.0011	1.136
4	$^{r}R_4(4)$	34 721 013.9	34 721 012.4370 ± 0.0007	1.505
5	$^{r}R_5(5)$	34 72 5080.3	34 725 074.8574 ± 0.0006	5.470
6	$^{r}R_6(6)$	34 729 147.3	34 729 149.9446 ± 0.0005	−2.633
7	$^{r}R_7(7)$	34 733 247.0	34 733 244.9299 ± 0.0006	2.044
8	$^{r}R_2(3)$	34 735 062.8	34 735 060.0431 ± 0.0026	2.773
9	$^{p}Q_3(4)$	34 736 831.9	34 736 828.9994 ± 0.0017	2.892
			34 736 830.7659 ± 0.0017	1.126
			34 736 832.5359 ± 0.0029	−0.644
10	$^{r}R_8(8)$	34 737 367.6	34 737 368.5083 ± 0.0006	−0.887
11	$^{r}Q_3(5)$	34 738 549.4	34 738 540.8459 ± 0.0009	8.557
			34 738 550.2162 ± 0.0014	−0.813
			34 738 559.5832 ± 0.0008	−10.180
12	$^{r}R_3(4)$	34 739 579.8	34 739 577.9827 ± 0.0012	1.807
13	$^{r}R_9(9)$	34 741 532.6	34 741 530.7673 ± 0.0008	1.870
–	$^{r}R_{40}(64)$	not measured	34 742 646.8843 ± 0.0020	–
14	$^{q}R_{36}(38)$	34 743 190.8	34 743 208.7755 ± 0.0027	−17.986
			34 743 215.9818 ± 0.0030	−25.192
			34 743 223.1982 ± 0.0026	−32.409
			34 743 185.0479 ± 0.0011	5.742
15	$^{r}R_4(5)$	34 744 132.1	34 744 130.5099 ± 0.0012	1.628
16	$^{r}R_{10}(10)$	34 745 730.9	34 745 717.9067 ± 0.0009	13.024
			34 745 743.5605 ± 0.0014	−12.629

Fig. 4(b) shows the fit residuals relative to the different WM signals corresponding to the $^{r}R_{40}(64)$ transition. It is worth noting that there is no evidence of etalon effects in the residuals and the best SNR ratio of 34 dB (30-ms lock-in integration time) is obtained for a CHF_3 pressure of 1 Pa. Also, some structures around the line center are observed regardless of the gas pressure. This could be ascribed to the additional complexity of the WM analysis to take into account modulation-induced line-profile distortions [11].

From the fitting analysis of the WM signals reported in Fig. 4, the line-center frequency of the $^{r}R_{40}(64)$ transition, extrapolated at zero pressure, is $(34\,742\,646\,884.3 \pm 2.0)$ kHz, which turns out to be in a fair good agreement with our previous determinations of the same transition, $(34\,742\,647.0 \pm 0.1)$ MHz [6] and $(34\,742\,646.96 \pm 0.02)$ MHz [14] (in both cases, the gas pressure and the pump power were 6 Pa and 5.0 mW, respectively), but with a type A (statistical) uncertainty at least ten times better. By repeating these measurements for different CHF_3 pressures, saturating pump powers, modulation frequencies and depths, the sensitivity coefficients of the $^{r}R_{40}(64)$ line-center frequency are also evaluated in order to quantify the main sources of systematic (type B) uncertainty. These are listed in Table 1, leading to an overall type B uncertainty of 400 Hz, 1×10^{-11} in fractional terms, slightly lower than the 2-kHz statistical contribution. The main systematic contributions are respectively due to the pressure reading accuracy of the adopted calibrated ceramic sensor (5% around 1 Pa) and the beam steering misalignment effects inside the gas cell that slightly shift the Lamb-dip center frequency [15].

With the same procedure and operating parameters (1 Pa CHF_3 pressure, 1.2 mW pump beam power) but with a slightly longer lock-in integration time of 100 ms, the absolute center frequency values of as many as 58 lines are measured and compared to those obtained by S. Albert and co-workers [1], using a FTIR spectrometer with a frequency resolution of 0.001 cm^{-1} (30 MHz). The results are summarized in Table 2. The type A (statistical) uncertainty of these line-center frequencies range from 0.4 to 3 kHz (from 1×10^{-11} to 9×10^{-11} in fractional terms) essentially set by the SNR of the WM detection scheme, which increases with the line intensity of the investigated transition, as it can be clearly observed in Figs. 5–7. Table 2 also reports the discrepancy between the line-center frequencies reported in [1] and those measured in this work: a mean frequency deviation of 0.851 MHz, with a standard deviation of 5.586 MHz, is found. In particular, thanks to the high-resolution capabilities of our sub-Doppler spectrometer ($\sim$55 kHz due to 50-kHz comb-tooth linewidth and $\sim$20-kHz transit-time line-broadening contributions), in Figs. 5–7 it is possible to appreciate how several lines, observed as isolated in [1], are actually composed by the superposition of distinct lines with a frequency separation lower than the $\sim$51-MHz Doppler linewidth (Table 3).

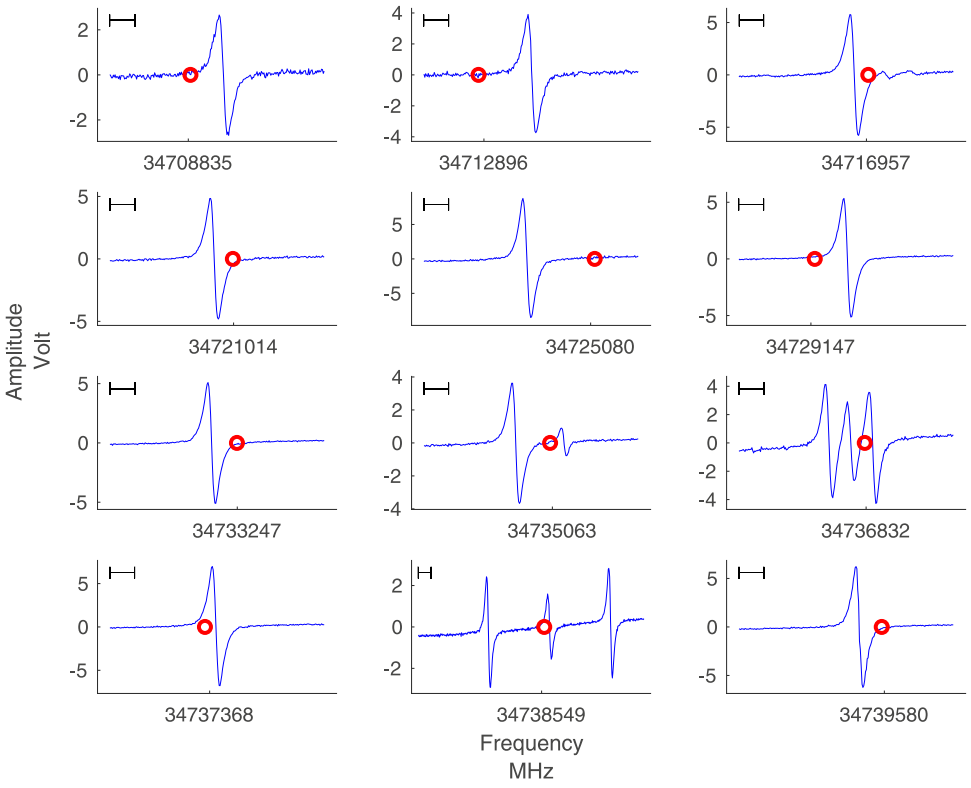

Fig. 5. First harmonic demodulated signal corresponding to the lines marked in Table 2 from 1 to 12, recorded for a saturating pump power of 1.2 mW and a CHF_3 pressure of 1 Pa (lock-in integration time 100 ms). The red circles represent the values measured in [1] and the horizontal bars correspond to a 2-MHz frequency span.

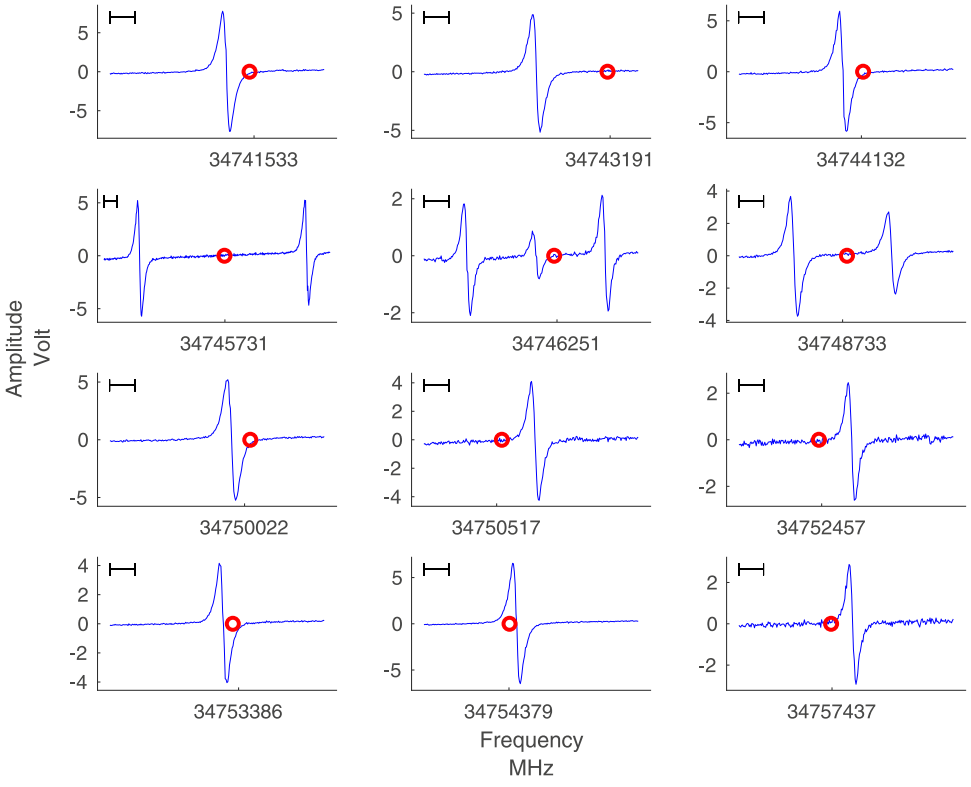

Fig. 6. First harmonic demodulated signal corresponding to the lines marked in Table 2 from 13 to 24. The measuring conditions are the same as in Fig. 5. Again, the red circles represent the values measured in [1] and the horizontal bars correspond to a 2-MHz frequency span.

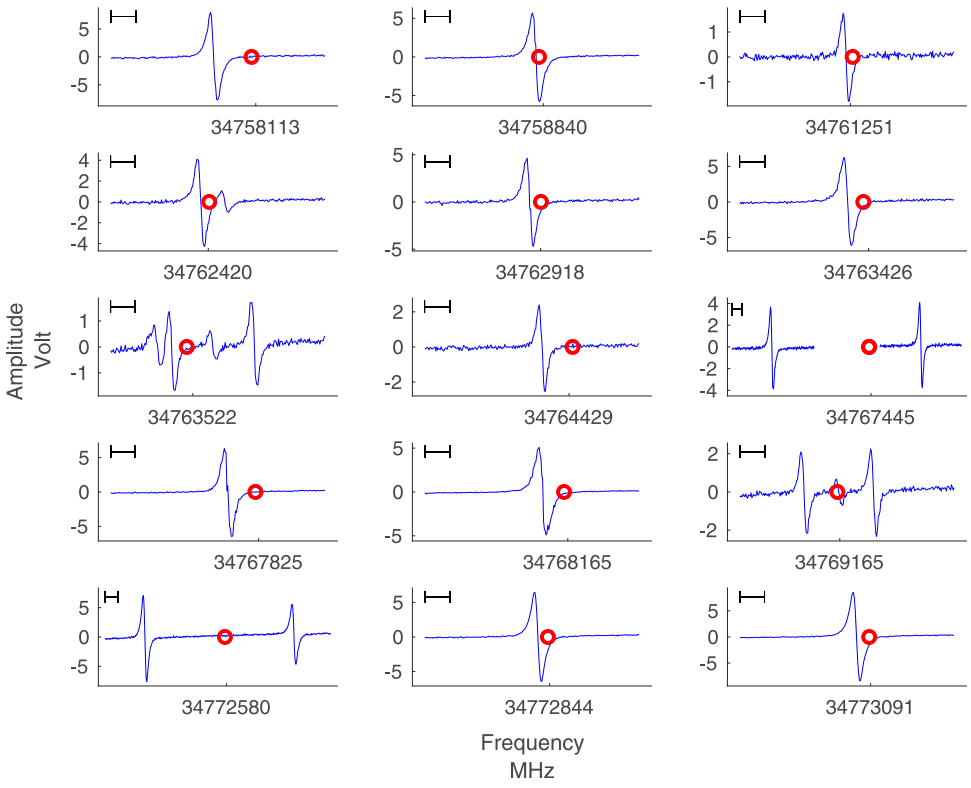

Fig. 7. First harmonic demodulated signal corresponding to the lines marked in Table 2 from 25 to 39. The measuring conditions are the same as in Fig. 5. Again, the red circles represent the values measured in [1] and the horizontal bars correspond to a 2-MHz frequency span.

Table 3
Absolute center frequencies of several ro-vibrational lines in the CHF_3 υ_5 band, measured for a gas pressure of 1 Pa and pump power of 1.2 mW. Comparison is made with the values measured with a frequency resolution of 30 MHz by S. Albert and co-workers for a gas pressure of 5 Pa [1]. The reported uncertainties correspond to the type A statistical contribution (1-sigma) that has to be combined with an estimated type B uncertainty on the order of 400 Hz (as deduced by Table 1).

	Line	FTIR [1] (MHz)	This work (MHz)	FTIR - this work (MHz)
17	$^{p}Q_3(8)$	34 746 250.8	34 746 243.7368 ± 0.0022	7.034
			34 746 249.3207 ± 0.0025	1.450
			34 746 254.8809 ± 0.0014	−4.110
18	$^{r}R_5(6)$	34 748 733.4	34 748 729.0657 ± 0.0014	4.287
			34 748 736.9559 ± 0.0011	−3.603
19	$^{r}R_{11}(11)$	34 750 022.5	34 750 020.9530 ± 0.0010	1.507
20	$^{r}R_0(2)$	34 750 517.4	34 750 520.0922 ± 0.0013	−2.675
21	$^{r}R_1(3)$	34 752 456.8	34 752 459.4223 ± 0.0017	−2.648
22	$^{r}R_6(7)$	34 753 385.5	34 753 384.7613 ± 0.0009	0.771
23	$^{r}R_{12}(12)$	34 754 379.0	34 754 379.6108 ± 0.0010	−0.567
24	$^{r}R_2(4)$	34 757 436.9	34 757 438.6647 ± 0.0015	−1.738
25	$^{r}R_7(8)$	34 758 112.7	34 758 109.6132 ± 0.0009	3.046
26	$^{r}R_{13}(13)$	34 758 839.7	34 758 839.4008 ± 0.0010	0.255
27	$^{p}Q_4(18)$	34 761 251.2	34 761 250.6489 ± 0.0021	0.538
28	$^{r}R_3(5)$	34 762 420.1	34 762 419.3883 ± 0.0030	0.689
29	$^{r}R_8(9)$	34 762 918.0	34 762 917.1283 ± 0.0016	0.904
30	$^{r}R_{14}(14)$	34 763 425.6	34 763 424.3134 ± 0.0010	1.268
31	$^{p}Q_3(12)$	34 763 521.5	34 763 519.1044 ± 0.008	2.410
			34 763 520.3190 ± 0.003	1.196
			34 763 523.6288 ± 0.007	−2.114
			34 763 526.9831 ± 0.0025	−5.468
32	$^{p}Q_4(9)$	34 764 429.3	34 764 426.8173 ± 0.0018	2.469
33	$^{r}R_4(6)$	34 767 444.6	34 767 424.0222 ± 0.0014	20.577
			34 767 455.5706 ± 0.0013	−10.972
34	$^{r}R_9(10)$	34 767 824.7	34 767 822.4955 ± 0.0018	2.240
35	$^{r}R_{15}(15)$	34 768 164.7	34 768 162.9665 ± 0.0017	1.734
36	$^{p}Q_3(13)$	34 769 164.8	34 769 162.1179 ± 0.0018	2.690
			34 769 164.9234 ± 0.007	−0.115
			34 769 167.7264 ± 0.0019	−2.918
37	$^{r}R_5(7)$	34 772 579.7	34 772 567.4563 ± 0.0006	12.288
			34 772 590.3380 ± 0.0010	−10.594
38	$^{r}R_{10}(11)$	34 772 843.9	34 772 843.0484 ± 0.0005	0.813
39	$^{r}R_{16}(16)$	34 773 090.9	34 773 089.8611 ± 0.0004	1.029

4. Conclusions

We reported on high-resolution and high-accuracy spectroscopic investigation of a wide portion of the CHF_3 υ_5 fundamental band around 8.6 μm using a metrological-grade frequency-comb-locked QCL. The absolute line center frequencies of 59 lines were measured with a fractional uncertainty ranging from 9×10^{-11} to 2×10^{-11}, which represents a two-order-of-magnitude improvement with respect to our previous studies. In addition, a detailed comparison with recent high-resolution FTIR measurements was also accomplished, bringing out an enhancement in the accuracy performance by more than three orders of magnitude. In conclusion, the availability of such ultra-accurate line-center frequency values for a large number of ro-vibrational transitions in the υ_5 fundamental band will allow a better understanding of the energy level structure of CHF_3 molecule.

Declaration of Competing Interest

The authors declare that they have no known competing financial interests or personal relationships that could have appeared to influence the work reported in this paper.

References

[1] Albert S, Bauerecker S, Bekhtereva ES, Bolotova IB, Hollenstein H, Quack M, Ulenikov ON. High resolution FTIR spectroscopy of fluoroform $^{12}CHF_3$ and critical analysis of the infrared spectrum from 25 to 1500 cm^{-1}. Mol Phys 2018;116(9):1091–107.

[2] Flaud JM, Orphal J. Handbook of high-resolution spectroscopy. In: Spectroscopy of the Earth's atmosphere. NY: John Wiley & Sons, Ltd, Chichester; 2011. p. 1971–92. 3, Chap.

[3] Albert S, Albert KK, Hollenstein H, Tanner CM, Quack M. Handbook of high-resolution spectroscopy. In: Fundamentals of Rotation-Vibration Spectra. Chichester, NY: John Wiley & Sons, Ltd; 2011. p. 117–73. 1, Chap.

[4] Quack M. IR Laser chemistry. Infrared Phys Technol 1995;36(1):365–80.

[5] Sommer C, van Buuren LD, Motsch M, Pohle S, Bayerl J, Pinkse PWH, Rempe G. Continuous guided beams of slow and internally cold polar molecules. Faraday Discuss 2009;142:203–20.

[6] Vicentini E, Gambetta A, Coluccelli N, Fasci E, Castrillo A, Gianfrani L, Sarno VD, Maddaloni P, Ceausu-Velcescu A, De Natale P, Wang Y, Fernandez TT, Laporta P, Galzerano G. Rovibrational fine structure and transition dipole moment of CF_3h by frequency-comb-assisted saturated spectroscopy at 8.6 μm,. J Quant Spectrosc Radiat Transf 2018;217:373–9.

[7] Gambetta A, Coluccelli N, Cassinerio M, Gatti D, Laporta P, Galzerano G, Marangoni M. Milliwatt-level frequency combs in the 8–14 μm range via difference frequency generation from an er:fiber oscillator. Opt Lett 2013;38(7):1155–7.

[8] Gambetta A, Cassinerio M, Coluccelli N, Fasci E, Castrillo A, Gianfrani L, Gatti D, Marangoni M, Laporta P, Galzerano G. Direct phase-locking of a 8.6-μm quantum cascade laser to a mid-IR optical frequency comb: application to precision spectroscopy of N_2O. Opt Lett 2015;40(3):304–7.

[9] The. characterization of the rb-reference was performed at the italian metrological institute (INRIM) with respect the Italian primary frequency standard based on a nitrogen-cooled cesium fountain clock (fractional accuracy 2×10^{-16}).

[10] Moses EI, Tang CL. High-sensitivity laser wavelength-modulation spectroscopy. Opt Lett 1977;1(4):115–17.

[11] Kluczynski P, Gustafsson J, Lindberg M, Axner O. Wavelength modulation absorption spectrometry — an extensive scrutiny of the generation of signals. Spectrochim Acta Part B 2001;56(8):1277–354.

[12] Westberg J, Wang J, Axner O. Fast and non-approximate methodology for calculation of wavelength-modulated voigt lineshape functions suitable for real–time curve fitting. J Quant Spectrosc Radiat Transf 2012;113(16):2049–57.

[13] Schilt S, Thevénaz L, Robert P. Wavelength modulation spectroscopy: combined frequency and intensity laser modulation. Appl Opt 2003;42(33):6728–38.

[14] Gambetta A, Vicentini E, Coluccelli N, Wang Y, Fernandez TT, Maddaloni P, De Natale P, Castrillo A, Gianfrani L, Laporta P, Galzerano G. Versatile mid-infrared frequency-comb referenced sub-doppler spectrometer. APL Photon 2018;3:046103.

[15] Bloemberger N, Chebotayev VP, Hall JL, Haroche S, Jacquinot P, Letokhov VS, Levenson MD, Magyar JA, Shimoda K. High-resolution laser spectroscopy. In: Shimoda K, editor. Saturation spectroscopy. Berlin Heidelberg: Springer; 1976. p. 95–171. chap. 4